# Energetics of Polar and Nonpolar Facets of PbSe Nanocrystals from Theory and Experiment

Changming Fang,[†,‡] Marijn A. van Huis,[†,*] Daniël Vanmaekelbergh,[§] and Henny W. Zandbergen[†]

[†]Kavli Institute of Nanoscience, Delft University of Technology, Lorentzweg 1, NL-2628 CJ Delft, The Netherlands, [‡]Materials Innovation Institute M2i, Mekelweg 2, NL-2628 CD Delft, The Netherlands, and [§]Debye Institute for NanoMaterials Science, Utrecht University, Princetonplein 1, NL-3508 TH Utrecht, The Netherlands

**ABSTRACT** Surface energies of the distinct facets of nanocrystals are an important factor in the free energy and hence determine the nanocrystal morphology, chemical and physical properties, and even interparticle dipole interactions. Here we investigate the stability and atomic structure of polar and nonpolar PbSe surfaces by combining first-principles calculations with high-resolution transmission electron microscopy (TEM). For uncapped surfaces, the calculations predict that the nonpolar {100} surface is the most stable with a surface energy of 0.184 J m$^{-2}$, while the nonpolar {110} and reconstructed {111}-Pb surfaces have surface energies of 0.318 J m$^{-2}$ and 0.328 J m$^{-2}$, respectively. Fully polar {111} surfaces are structurally unstable upon relaxation. These findings are in good agreement with TEM observations showing that capped nanocrystals have a nearly spherical, multifaceted morphology, while cubical shapes with predominantly {100} facets are obtained when the capping molecules are removed through heating in vacuum. During this process, however, also multipolar surfaces can temporarily exist just after the removal of the surfactants. These metastable {111} surfaces consist of ribbon-like nanodomains, whereby the ribbons are alternating in polarity. The calculations confirm that these multipolar surfaces are energetically more favorable than fully polar surfaces. The consequences for capped nanocrystals (a dominant Pb-oleate termination) and nanocrystal fusion (a shorter interaction range of dipole interactions) are discussed.

**KEYWORDS:** nanocrystals · surface energies · polar surfaces · transmission electron microscopy · first-principles calculations

Many chemical and physical processes and properties, such as crystal growth, crystal morphology, and adsorption, are controlled by the atomic structure of the surface and its energy. This is even more important for nanostructured materials, in which the surface energy gives a considerable contribution to the total energy. Knowledge of the surface structures and energies allows predicting and optimizing the synthesis and, eventually, processing of nanocrystals into genuine nanomaterials. In recent years, PbSe nanomaterials have been intensively studied because of their attractive physical properties and promises for near-infrared opto-electronic applications.[1−9] Through fusion of smaller nanocrystal units, larger nanostructures can be fabricated with a wide variety of single crystal morphologies, such as nanorods, spheres, cubes, stars, and rings.[1,10−15] The experiments suggest that the efficient oriented attachment—the mutual alignment of nanocrystals during or prior to fusion—can be attributed to dipole interactions caused by the electrically charged, Pb- or Se-terminated {111} facets.[10,12−15] However, this is currently just a hypothesis. Although it is experimentally proven that the nanocrystals carry dipole moments,[16,17] the experiments are not sufficiently sophisticated to prove the presence of nonreconstructed, fully polar {111} facets, and theoretical investigations are absent.

There are many experimental and theoretical studies on the properties of bulk PbSe,[18−22] while the literature on the surface structure and energy is scarce. Kimmura et al.[23] grew a PbSe {111} surface on the {111} surface of BaF$_2$. From the results of the high-resolution Rutherford backscattering spectroscopy, they found that the PbSe {111} surface is dominated by Pb atoms.

Moreels and co-workers prepared colloidal PbSe nanocrystals of a uniform size.[24] They also investigated the interplay between the Pb-coordinating ligands and the structure of the PbSe surfaces in solution by nuclear magnetic resonance spectroscopy (NMR). It was concluded that the ligands have a strong impact on the nanocrystal surfaces and that capped PbSe nanocrystals are nonstoichiometric with a surface that is composed mainly of oleic acid capped lead atoms.[24] Ma et al. investigated the geometric and electronic properties of PbX (X = S, Se, and Te) {100} surfaces using the density functional method.[25] However, there is no information about the surface energies.

With the fast increasing interest in colloidal semiconductor nanocrystals, it is of key importance to investigate the surface structures and related energies of colloidal PbSe
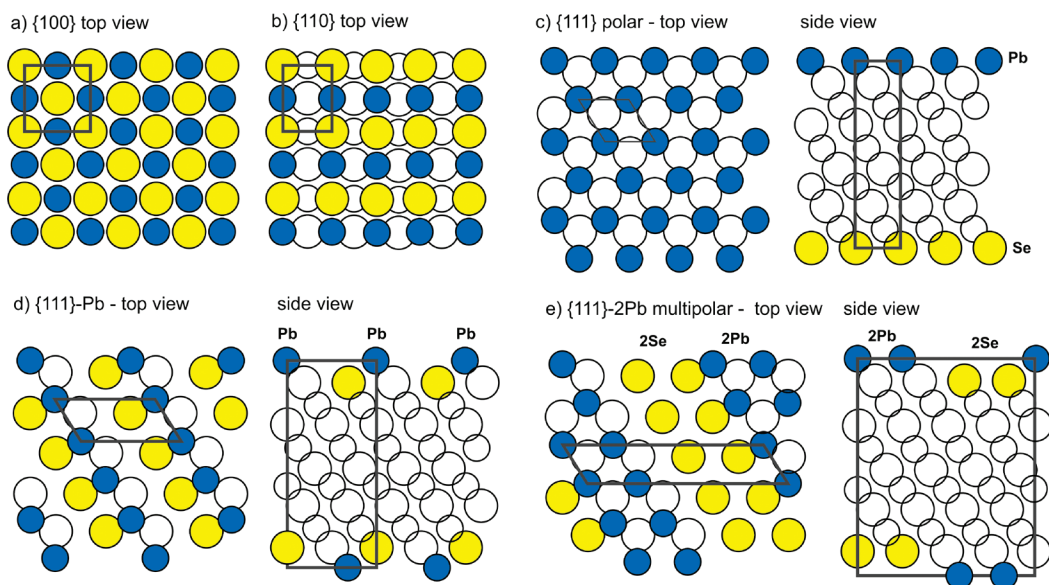
**Figure 1. Configuration of {100}, {110}, and {111} PbSe surfaces.** Full circles indicate surface atoms (top layer) and quasi-surface atoms (these atoms are only partially covered; they have at most one atomic bond to the top layer). Empty circles indicate subsurface atoms (having two or more bonds with atoms at an elevated layer). Subfigure (c) shows a fully polar configuration with one Pb-terminated surface and one Se-terminated surface in order to maintain stoichiometry. The bottom two configurations (d,e) are reconstructed {111} surfaces. There is one reconstructed variant {111}-Pb whereby half the Pb atoms are absent in the surface layer, and a domain-wise polar variant {111}−2Pb with ribbons of Pb atoms on top of a Se atomic layer. {111}-Se and {111}−2Se surfaces can be constructed analogously.

nanocrystals, a prototype of a NaCl-type crystal, optically active in the near-infrared. Here, we present both theoretical (density functional theory (DFT) simulations) and experimental (transmission electron microscopy (TEM)) results on the different surfaces of PbSe. The obtained information is not only helpful to understand the stability of nanocrystalline facets, but also to understand the difference between capped and uncapped nanocrystals, and temperature-induced nanocrystal reconstructions.[4,10,26,27] In the case of nanometer-sized crystals, the relative occurrence of different facets is determined by the surface energies. The relative surface energies can be obtained by analysis of HRTEM data of the nanocrystals, using the Wulff diagram.[28,29]

For the experiments, PbSe nanocrystals were used with sizes of 8.0 and 9.8 ± 0.7 nm in diameter; the original oleic acid capping is replaced by hexylamine capping in order to obtain uncapped nanocrystals by molecular evaporation at relatively low temperature. Details on the synthesis are given elsewhere.[30] The TEM specimens were prepared by drop-casting PbSe NC suspensions in toluene on a SiN MEMS microhotplate with electron-transparent windows, which allows high-resolution imaging at elevated temperature.[15] A Titan aberration-corrected microscope operating at 300 kV was used for TEM characterization of the nanocrystals. To investigate the stability of the polar {111} facets and to observe changes in morphology of the nanocrystals, the nanocrystals were heated at temperatures up to 150 °C.

Below we will first discuss the structure of the polar and nonpolar surfaces of PbSe, followed by the experimental TEM results and the theoretical density func-

tional theory (DFT) calculations. Next, experimental and theoretical findings of an unusual reconstruction of the polar {111} surfaces are discussed, followed by a brief summary of the conclusions.

## RESULTS AND DISCUSSION

**Polar and Nonpolar PbSe Surfaces.** To calculate the energies of various PbSe surfaces using quantum mechanical methods, appropriate supercells need to be constructed which are always stoichiometric and periodic in three dimensions. These cells include two surfaces, separated by a slab of vacuum thick enough to render the interaction between the surfaces negligible. Two such supercells are shown in the Supporting Information.

Figure 1 shows all the PbSe surfaces considered in this work. PbSe has the cubic rock salt or NaCl-type structure[31] with one lattice parameter $a_0$. The presently calculated lattice parameter ($a_0 = 0.621$ nm) is slightly larger than the experimental values ($a_0 = 0.610$ nm at 40 K and $a_0 = 0.612$ nm at room temperature),[16,20,31] which is not untypical for the DFT-GGA methods (computational details are given in the Methods section). Our calculated value is also close to the former theoretical calculations ($a_0 = 0.611$ nm, or $a_0 = 0.621$ nm).[19,20] In the bulk structure, each atom has six nearest neighbors in the direction of the cubic ⟨100⟩ axes. Each Pb atom has six Se atoms as nearest neighbors, and each Se atom has six Pb nearest neighbors.

At the {100} surface, each atom misses one nearest neighbor (see Table 1 and Figure 1a). The unit cell of the {100} surface has an area of $a_0 \times a_0$ ($a_0$ is the lat-

**TABLE 1. Cleavage and Surface Energies for the Low-Index Surfaces of PbSe Using the DFT-GGA-PAW Method[a]**

| surfaces | broken bonds (per atom) | | $\gamma_{cleav}$ (J m$^{-2}$) | $\gamma_{surface}$ (J m$^{-2}$) |
|---|---|---|---|---|
| (100) | Sf (Pb,2/4): | 1 | 0.488 | 0.184 |
| | Sf (Se,2/4): | 1 | | |
| (110) | Sf (Pb,1/2): | 2 | 0.983 | 0.318 |
| | Sf (Se,1/2): | 2 | | |
| (111)-a fully polar | Sf (Pb,3/3): | 3 | unstable[b] | unstable[c] |
| | Sf (Se,3/3): | 3 | unstable[b] | unstable[c] |
| (111)-Se nonpolar | Sf (Se,2/4): | 3 | 1.493 | 0.419 |
| | Ssf (Pb,2/4): | 1 | | |
| | Ssf (Pb,2/4): | 2 | | |
| (111)-Pb nonpolar | Sf (Pb,2/4): | 3 | 1.367 | 0.328 |
| | Ssf (Se,2/4): | 1 | | |
| | Ssf (Se,2/4): | 2 | | |
| (111)-2Pb nanopolar | Sf. (Pb,2/4): | 3 | 1.634 | 0.412 |
| | Ssf.(Se,1/4): | 3 | | |
| | Ssf.(Se,1/4): | 2 | | |
| | Ssf.(Se,1/4): | 1 | | |
| | Ssf.(Se,1/4): | 0 | | |

[a]The surface configurations are shown in Figure 1. In the second column, the number of broken bonds for the surface (and subsurface) atoms are also given. Here Sf represents the surface atomic layer (AL) and Ssf the sub-surface AL. In between brackets, the number of the Pb and Se atoms are given with respect to the total number of atoms in the AL. [b]The cleavage energy depends on the shapes and thickness of the slab and vacuum. [c]The two top surface layers detach and are displaced into the vacuum during the structural relaxation.

tice parameter of the bulk), each atomic layer (AL) in the cell contains two Pb and two Se atoms. The c-axis contains a PbSe slab of 2.48 nm and a vacuum layer of 1.24 nm.

The {110} surface unit cell displayed in Figure 1b has an area of $\sqrt{2}a_0 \times a_0$. Each AL contains equal numbers of Pb and Se atoms, and the Pb and Se atoms form lines along the a-axis. The atoms at the surface layer miss two nearest neighbors. The supercell has a length of about 3.51 nm (about 1.76 nm slab and 1.76 nm vacuum).

The polar {111} surface is shown in Figure 1c. The stacking order along the ⟨111⟩ axis is ...AcBaCb..., whereby A,B,C represent Pb atoms and a,b,c represent Se atoms. Therefore, the {111} atomic layers consist entirely of either Pb or Se atoms and are alternating as ...PbSePbSePbSe... The structure can be described by a hexagonal lattice ($a = \sqrt{2}a_0$) as displayed in Figure 1c, whereby each AL contains one Pb or Se atom in the unit cell. PbSe is an ionic material whereby the Pb and Se atoms carry positive and negative charges, respectively. Because the atomic layer at the surface consists entirely of Pb or Se atoms, the top layer contains a net charge which leads to an electric dipole moment in the direction perpendicular to the surface. Such polar surfaces are not stable for large crystal sizes.[32−34]

To investigate feasible {111} surfaces, defective surfaces need to be constructed, as in the cases of oxides.[32−34] We create a configuration starting from the smooth, fully polar {111} surface displayed in Figure 1c. Here the slab has two fully occupied surfaces, that is,

one surface contains only Pb atoms and the other only Se atoms. Half the Pb atoms from the Pb top layer are moved to the other side of the slab, and added in the empty Pb layer on top of the Se surface layer, as shown in Figure 1d. We refer to this reconstructed surface as {111}-Pb. Both surfaces in the calculation cell are now equivalent and partially Pb-terminated. {111}-Se reconstructed surfaces can be constructed analogously. The thickness of the slab is 3.18 nm and the vacuum between the surfaces is 1.12 nm. The systems are stoichiometric and the surfaces are nonpolar. Although the partially occupied top layer contains net charge, the fully occupied Pb/Se layers underneath contain alternating opposite charges twice as large, which renders the net dipole moment perpendicular to the surface very small; Therefore, we consider these reconstructed {111}-Pb and {111}-Se surfaces nonpolar.

For the smooth {111} surfaces, each surface atom misses three nearest neighbors. Meanwhile, for the defective {111} surfaces, each surface atom in the partially occupied top layer loses three nearest neighbors. Of the subsurface atoms, half are four-coordinated (three bonds in the slab and one bond with the surface atom) while the other half are five-coordinated (three bonds in the slab and two bonds to the surface atoms). The total number of broken bonds for a defect surface is the same as for a smooth surface, as shown in Table 1.

All calculations were performed for PbSe surfaces without capping molecules. In the TEM analysis, the morphology of nanocrystals with and without capping molecules is investigated and mutually compared.

**Experimental TEM Analysis of PbSe Nanocrystals.** To investigate the difference in morphology between hexylamine-capped and uncapped nanocrystals, PbSe NCs were first dropcast onto a thin SiN membrane, and subsequently heated in situ in the TEM to remove the hexylamine capping through evaporation. For this purpose, it was necessary to replace the original oleic acid capping with hexylamine, because heating with the original oleic acid capping leads to carburization of not-evaporated ligands, which hampers a reliable NC surface analysis (details are in the Supporting Information). It is known from previous work that the nanoclusters have a tendency to fuse to larger single crystals when temperatures of 100−150 °C are reached.[15] In this work, the NCs were first analyzed as dropcast and were subsequently heated at a rate of 3.3 °C/s from room temperature to 120 °C, after which the temperature was kept constant. After 30 min at this temperature, the nanoclusters were analyzed again and were found to have transformed into cubical shapes as described into more detail below. Heating in the same way to a higher temperature of 150 °C gave the same result.

Below certain NC sizes, size effects may change the equilibrium morphology. In this work, two nanocrystal sizes of 8.0 and 9.8 ± 0.7 nm were used and no difference in morphology evolution was found, which
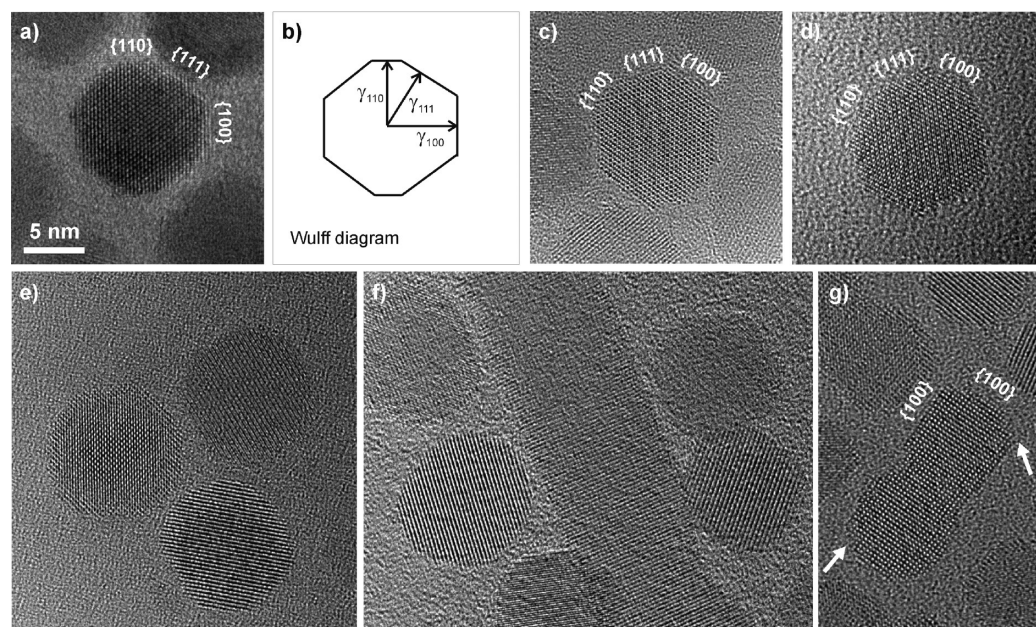
**Figure 2. High-resolution TEM images showing the morphology of PbSe NCs:** (a) PbSe nanocrystals in a [011] projection, so that the {100}, {110}, and {111} surfaces can be observed simultaneously; (b) example of the Wulff diagrams (in this case corresponding to panel a) that were used to derive relative surface energies; (c,d) other PbSe NCs in a [011] projection; (e) other NCs in various orientations; (f) nanowires are formed in low-density areas after annealing at 120 °C; (g) in general, cubical shapes start to dominate after longer annealing times as the surfactants evaporate; the corners of the cubes display {100} nanofaceting, as indicated with white arrows.

suggests that size effects are not significant for PbSe in this size range.

Figure 2a–e shows the morphology of PbSe nanocrystals (NCs) as dropcast from the suspension. The surface Pb atoms are for a great part bond to hexylamine, which forms the capping ligand of the nanocrystals. When in the right orientation, {100}, {110}, and {111} facets can be distinguished. Upon annealing, the hexylamine evaporates from the nanocrystals leaving virgin facets, some of these having a high energy. Hence, nanocrystal reconstructions are induced to lower the overall energy. For instance, upon annealing at a temperature of 120 °C, nanowires are formed (Figure 2f) from individual NCs due to oriented attachment.[15] Here, we focus on the surface reconstructions observed with individual PbSe nanocrystals.

Isolated nanocrystals that have a nearly spherical, multifaceted morphology become increasingly cubic after decapping. The corners of the cubes are imperfect, but do not correspond to {110} nor to {111} facets which are commonly found in the capped nanocrystals. Cubical shapes are clearly observed in Figure 3, where larger PbSe crystals are displayed that were formed from fusion of smaller NCs after extended annealing at 150 °C. Figures 2g and 3 show that the corners of the nanocrystals are reconstructed into tiny {100} facets, indicating that {100} is the most stable surface. Figure 4 shows the ideal configuration of uncapped nanocrystals, and the evolution from multifaceted, capped surfaces to reconstructed, {100} nanofaceted surfaces. The nanocrystal morphology, the relative area of the different facets and the associated surface energy all change during the annealing treatment. Of key importance here is the influence of the hexylamine capping. The polar heads of these ligands can stabilize (polar) facets that are unstable when the original oleic acid capping is removed.

The Wulff diagram[28,29] was used to deduce the ratio of the surface energies from the nanocrystal morphology. As an example, Figure 2b shows the Wulff diagram derived from the experimental image 2a, showing a capped nanocrystal displaying {100}, {110}, and {111} surfaces (in the [011] projection, all relevant surfaces are
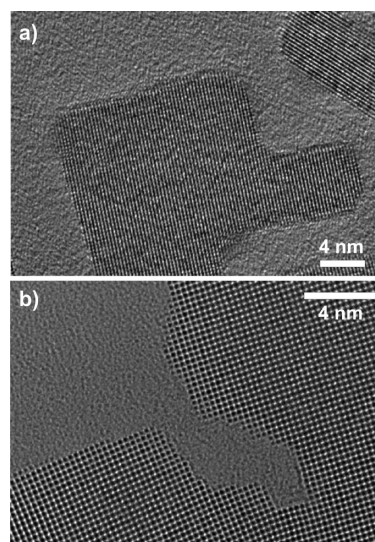


**Figure 3. Large crystals of PbSe obtained after extended annealing at 150 °C:** (a) large rectangular PbSe nanocrystal; (b) surfaces that have reconstructed into nonpolar {100} nanofacets, as schematically shown in Figure 4d.
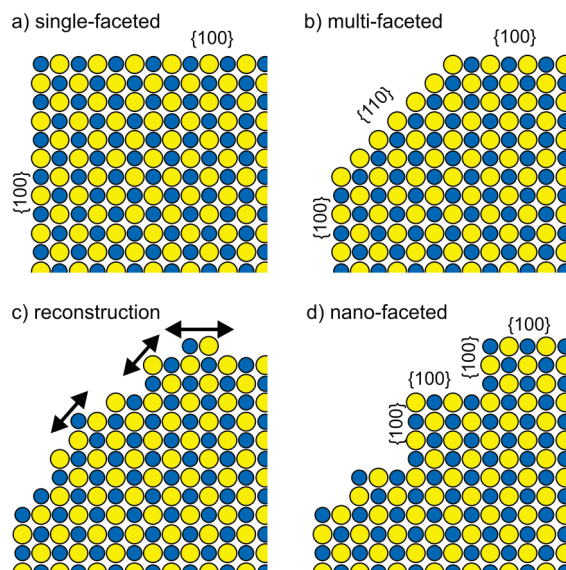
Figure 4. Schematic showing the surface configuration of (a) an ideal single-faceted nanocrystal having only {100} facets; (b) a multifaceted nanocrystal surface; (c) a reconstructing surface; and (d) a {100} nanofaceted surface.

present). In Figures 2g and 3 however, the surfactants are no longer present due to annealing and the nanocrystal shape transforms to a cube with dominant {100} surfaces. Table 2 lists the average relative surface energies that are derived experimentally applying the Wulff diagram for 20 surfactant-covered NCs (examples are in Figure 2a,c,d), as derived from the cubical shapes of surfactant-free nanocrystals (Figures 2g, and 3), and as deduced from the theoretical calculations (Table 1).

Because no calculations were performed on surfactant-covered surfaces, a direct comparison between theory and experiment cannot be made for that case. However, for uncapped surfaces the experimental values (derived from the cubical shapes and {100} nanofaceting) are in excellent agreement with the theoretical data. Here it should be realized that the Wulff diagram is a three-dimensional diagram. If the {110} and {111} surface energies are much higher than the {100} surface energy, the {110} and {111} surfaces in Figure 2b will be "pushed out" by the vectors with relative lengths $\gamma_{110}$ and $\gamma_{111}$, respectively, until the six {100} facets inter-

sect to form a cube. The {110} facets will no longer be present when their energy is higher than $\sqrt{2}\gamma_{100}$, and the {111} facets will no longer be present when their energy exceeds $\sqrt{3}\gamma_{100}$, hence the values of 1.41 and 1.73 in Table 2.

**Calculation of PbSe Surface Energies.** For all above-mentioned surfaces, both the cleavage and surface energies were calculated. The minimum energy to cleave a crystal is named the cleavage energy $\gamma_{cl}$, and is calculated as[32−34]

$$\gamma_{cl} = (E_{slab} - E_{bulk})/A \qquad (1)$$

where the $E_{slab}$ is the energy of the cleaved system, $E_{bulk}$ the cohesive energy of the bulk PbSe with the same number of atoms, and $A$ the area of the cleavage surface. In general such cleaved surfaces will relax or even reconstruct to a more stable surface structure with a different energy. The surface energy $\gamma_{surf}$ for each surface is then defined as[34]

$$\gamma_{surf} = (E_{relax} - E_{bulk})/2A \qquad (2)$$

One cleavage creates two surfaces, hence the factor 2 in eq 2 in comparison with eq 1. If there would be no reconstruction of the surfaces, the surface energy would be equal to half the cleavage energy; however, in general relaxation will always take place and lower the surface energy. The value of surface energy ($\gamma_{surf}$ with unit J m$^{-2}$) can be used to predict the stability of the surface. The larger the value is, the less stable is the surface. Table 1 lists calculated cleavage energies and surface energies, as well as details about the termination and the number of broken bonds.

First we discuss the cleavage energies of PbSe. Among the three low-index orientations, cleavage in the {100} plane requires the least energy, as shown in Table 1. On the other hand, the cleavage energies in {111} planes are significantly larger than those of the {100} and {110} planes. That agrees with experiments where it was found that the {100} plane is the cleavage orientation according to the Griffith's criteria.[35]

Structural relaxation of the {100} surface (Figure 1a) is moderate. The surface Pb/Se atoms move inward to the slab. The surface also becomes uneven, as the Pb atoms (0.019 nm) are displaced inward more than the Se atoms (0.016 nm). There is also a slight oscillation of the interlayer distances. These findings are similar to the recent calculations by Ma et al.[25] Comparatively, the structural relaxation of the {110} surface, displayed in Figure 1b, is much stronger. The relaxation occurs mainly in the direction perpendicular to the surface. The surface Se atoms move 0.005 nm outward, while the surface Pb atoms move 0.009 nm inward. As a result the Se atoms again are about 0.014 nm higher than the Pb atoms on the {110} surface.

**TABLE 2. Summary of Experimental and Theoretical Surface Energy Ratios**[a]

| surface energy ratio | as dropcast (capped) | after annealing (uncapped) | theory (Table 1) |
|---|---|---|---|
| $\gamma_{110}/\gamma_{100}$ | 1.00 | 1.00 | 1.00 |
| $\gamma_{110}/\gamma_{100}$ | 1.02 ± 0.03 | >1.41 | 1.73 |
| $\gamma_{111}/\gamma_{100}$ | 0.96 ± 0.02 | >1.73 | 1.78 |

[a]The averaged experimental values for as-dropcast NCs were determined from the relative size of the facets using Wulff diagrams (example in Figure 2b) of 20 NCs in a [011] projection (as in Figure 2a,c,d). The error is twice the standard deviation in the relative surface energies derived from the 20 NCs. The experimental ratio after extended annealing was deduced from the cubical shapes observed after extended annealing at 120 and 150 °C (Figures 2g and 3) as described in the text. Theoretical values for uncapped surfaces are derived from Table 1.

A smooth {111} system with one Pb-terminated surface and one Se-terminated surface, as displayed in Figure 1c, is structurally completely unstable. During structural relaxation, the two top layers ({···PbSe} at the one end of the slab and {···SePb} at the other end of the slab) detach from the surface and are displaced into the vacuum, followed by the detachment of the next bilayers, until the crystal has completely disintegrated. The smooth, polar {111} surfaces are therefore structurally unstable, and a meaningful surface energy cannot be calculated.

The *reconstructed* {111}-Pb and {111}-Se surfaces (Figure 1d) with half-occupied Pb or Se surface layers were found to be structurally stable, though. As explained previously, these reconstructed surfaces can be considered nonpolar because the net dipole moment at the surface is small. The structural optimizations showed strong relaxation, occurring mainly along the direction perpendicular to the surface. Details are given in the Supporting Information.

Our calculations show large differences between the energies of the different PbSe surfaces, as shown in Table 1. The {100} surface is the most stable one with the lowest surface energy of 0.184 J m$^{-2}$. The {110} surface has a surface energy 73% higher than that of the {100} surface. The calculated surface energies are in good agreement with the experimental observations and the Wulff model for the case of uncapped surfaces, that is, after the removal of the capping molecules through annealing (see Table 2). The surface energy of the reconstructed {111}-Pb surface is close to that of {110}, as shown in Table 1. The calculations also show that the {111}-Pb surface is significantly more stable than the {111}-Se surface (Table 1), indicating high stability of the Pb-terminated surfaces. This agrees with the preferred Pb-termination as found by means of Rutherford backscattering spectroscopy performed on epitaxially grown PbSe{111} layers.[23]

**Nanodomains on Multipolar {111} Surfaces.** We have described the theoretical and experimental results on the most obvious surface types. However, both during the experiments and when varying surface reconstructions in the calculations, we have found a strongly deviating {111} surface type which consists of nanodomains with alternating polarity, so that we can speak of a multipolar surface. Below we will first discuss the structure of that interface and its metastable energy, followed by the experimental TEM observation of that surface which exists only temporarily, shortly after removal of the capping molecules.

As previously mentioned, the calculations showed that the reconstructed nonpolar {111}-Pb surfaces have much lower surface energies than the fully occupied, polar {111} facets. However, alternative reconstructions with nanosized polar domains on {111} surfaces were found to be energetically favorable as well. Various possibilities for nanopatterning can be considered. To show the effect of charge-domains on the {111} surfaces, we build the following configuration. Starting from the reconstructed {111}-Pb surfaces, a supercell is built with an area of $4a_h \times a_h$ (with $a_h$ being the length of the $a$-axis of the hexagonal lattice), as shown in Figure 1e. In the unit cell, two Pb atoms occupy two neighboring sites while the other two sites are unoccupied to maintain the zero-charge nature of the surface. We therefore denote this surface as {111}-2Pb. As a result, the surface consists of alternating ribbons of Pb and Se atoms. The Se atoms in the sublayer have four different coordinations: one-quarter of them lose three Pb bonds (Se-3) as in the {111}-Se surface, one-quarter lose 2 Pb neighbors (Se-4), and one-quarter lose 1 Pb neighbor (Se-5), in the same way as in the case of the {111}-Pb surface. The last one-quarter of Se atoms are six-coordinated (Se-6).

The calculations show strong relaxation (or reconstruction) for the surface and subsurface atoms, although the basic structure is retained. The two Pb atoms in the top layer have total displacements of 0.022 and 0.026 nm, respectively, and form uneven ribbons. Details are given in the Supporting Information.

As shown in Table 1, the surface energy of the {111}-2Pb domain surface is 0.412 J m$^{-2}$, which is about 26% higher than that of the {111}-Pb surface, and slightly lower than that of the {111}-Se surface. Therefore, the calculations predict metastability of these charged {111} domains. Note that the calculations are for the ground state (at zero K and zero pressure). At higher temperatures, where entropy contributions are significant, the multipolar {111} domains can very well be energetically more favorable or even stable. The tiny polar domains also provide active sites for ligands, which further reduces the surface energy and makes their occurrence more probable. Considering that the Pb-ribbons are positively charged while the Se-ribbons are negatively charged, the nanodomains induce tiny dipoles on the {111} surfaces, which will induce interactions between nanocrystallites. During a heating experiment of PbSe NCs,[15] experimental evidence was found for the existence of such nanodomains.

Figure 5 shows a TEM image with a PbSe nanocrystal sticking out over the edge of a hole in the SiN membrane, with its {111} surface observed edge-on, at various instants in time. The TEM recordings were made at a temperature of 120 °C, so that the surfactants are no longer present. In Figure 5b, a three-dimensional schematic shows the corresponding nanopatterning which is based on the domain model displayed in Figure 1e. A continuous reconstruction of dipole nanodomains at the {111} surface is observed. The exposure time of the individual recordings was 200 ms, and changes of the surface (lateral displacement of individual rows) were observed multiple times per second. The transient nature of the surface is in agreement with the calculations predicting metastability of {111}-2Pb and {111}-Pb surfaces and instability of the smooth {111} surfaces.

As mentioned in the introduction, Moreels *et al.*[24] reported from NMR observations that the surfaces are mainly Pb-terminated and thus that the NCs are non-stoichiometric. Strictly speaking, the calculations performed in the current work are only valid for stoichiometric PbSe. However, it can be expected that the relative energies will be quite similar when the material is nearly stoichiometric. Qualitatively, the NMR observations can be related to our theoretical results as follows. We showed that nonreconstructed, fully polar Pb- or Se-terminated {111} surfaces are completely unstable. However, in a solution during nanocrystal synthesis, the Pb-terminated surfaces become capped with the capping ligand, while the Se atoms on the Se surface become covered with Pb-ligand moieties. In such a way, polar surfaces become predominantly Pb-ligand terminated.

We note that there should be a remarked difference between the electric interactions of fully polar surfaces and multipolar, nanodomain surfaces. The interaction force of multidipole surfaces is relevant at much shorter distance (the potential energy of linear multipoles decreases as $1/r^3$ or even faster) than for uniformly charged surfaces (where the Coulomb potential energy decreases with $1/r$).[36] So at a separation of, for example, 10 nm, the force between linear multipole facets will be about 100 times weaker than the force between uniformly charged facets. However, at sufficiently short distance the interaction between the {111} multidomain surfaces might still be sufficiently strong to explain the dynamics or oriented attachment, reported in a previous work.[15] Although the calculations were performed only for uncapped surfaces, it is likely that nanodomain-patterning is also favorable for the case of capped {111} surfaces, considering that the interface energy is the sum of the formation energy of the surface and the adhesion energy of the surfactants. The formation energy of the PbSe surface is lower, while the nanodomains are still large enough in area to have strong interactions with the capping molecules.

## CONCLUSIONS

By means of first-principles calculations, {100}, {110}, and {111}-Pb surface energies of PbSe were calculated as 0.184, 0.318, and 0.328 J m$^{-2}$, respectively. Fully polar surfaces are structurally unstable, and making the slab thin-
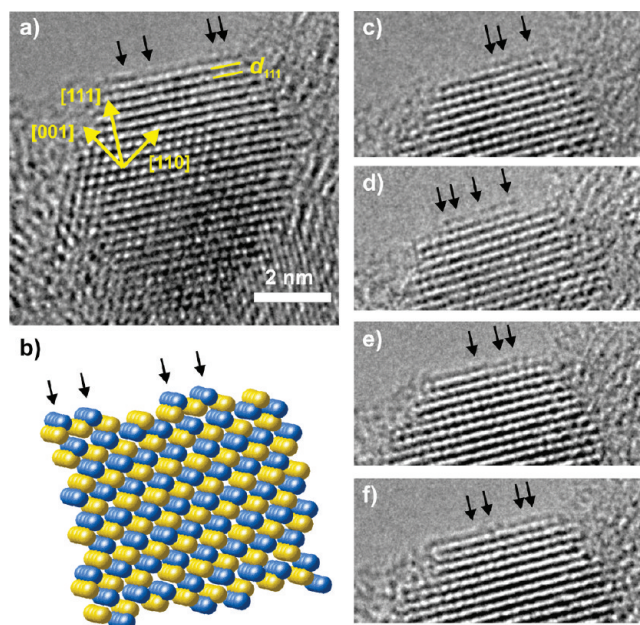


**Figure 5. Experimental evidence of nanodomains at the PbSe(111) surface. (a) TEM image of a PbSe nanocrystal with its (111) surface over the edge of the SiN support. (b) Three-dimensional schematic showing the nanopatterning based on the domain model. (c–f) Same as panel a, at various instants in time. Continuous reconstruction of polar nanodomains at the (111) surface is observed. The TEM recordings were made at a temperature of 120 °C, so that the surfactants (hexylamine) are no longer present.**

ner could not stabilize the surfaces. However, reconstructed {111} surfaces with ribbonlike polar domains can occur. The calculated results are in good agreement with TEM observations, where transitions in morphology were observed (from multifaceted nearly spherical to nearly cubic) as hexylamine surfactants are removed through gentle annealing. Although surfactants can substantially decrease the surface energy, the presence of fully polar {111} facets—which would induce very large dipole moments—is unlikely because Pb-terminated reconstructed {111} surfaces (both nonpolar and nanodomain polar) have formation energies an order of magnitude lower. Therefore, alternating negative/positive polar nanodomains can be stable on {111} facets. Consequently, dipole interactions between such nanocrystals—leading to efficient oriented attachment—are certainly possible, but the interaction range will be much shorter than is currently assumed in the literature.

## METHODS

All calculations were carried out using the first-principles' VASP code (Vienna *ab initio* Simulation Program)[37–39] employing the density functional theory (DFT) within the projector-augmented wave (PAW) method.[40,41] The generalized gradient approximation (GGA) digitalized by Perdew, Burke, and Ernzerhof (PBE) was employed for the exchange and correlation energy terms.[42] The cut-off energy of the wave functions and the augmentation functions is 264.4 and 446.8 eV, respectively. The electronic wave functions were sampled on a 12 × 12 × 12 grid with 84 *k*-points in the irreducible Brillouin zone (BZ) of bulk PbSe using the Monkhorst and Pack method.[43] The *k*-meshes of the surface systems were produced in cor-

respondence with that of the bulk. We tested different *k*-meshes (from 10 × 10 × 10 with 56 *k*-points to 20 × 20 × 20 with 285 *k*-points) for a conventional cell of bulk PbSe, as well as cutoff energies from 200 to 600 eV and from 400 to 700 eV for the waves and augmentation waves, respectively. The tests of *k*-mesh and cutoff energies showed a good convergence (<1 meV/atom).

*Supporting Information Available:* Details of supercells, structural relaxations, and ligand exchange. This material is available free of charge *via* the Internet at http://pubs.acs.org.

## REFERENCES AND NOTES

1. Yin, D.; Alivisatos, A. P. Colloidal Nanocrystal Synthesis and the Organic—Inorganic Interface. *Nature* **2005**, *437*, 664–670.
2. Zhu, T.; Berger, A.; Tan, Z. N.; Cui, D. H.; Xu, J.; Khanchaitit, P.; Wang, Q. Composition-Limited Spectral Response of Hybrid Photovoltaic Cells Containing Infrared PbSe Nanocrystals. *J. Appl. Phys.* **2008**, *104*, 044306.
3. Law, M.; Luther, J. M.; Song, O.; Hughes, B. K.; Perkins, C. L.; Nozik, A. L. Structural, Optical, and Electrical Properties of PbSe Nanocrystal Solids Treated Thermally or with Simple Amines. *J. Am. Chem. Soc.* **2008**, *130*, 5974–5985.
4. Kovalenko, M. V.; Talapin, D. V.; Loi, M. A.; Cordella, F.; Hesser, G.; Bodnarchunk, M. I.; Heiss, W. Quasi-Seeded Growth of Ligand-Tailored PbSe Nanocrystals through Cation-Exchange-Mediated Nucleation. *Angew. Chem., Int. Ed.* **2008**, *47*, 3029–3033.
5. Wang, R. Y.; Feser, J. P.; Lee, J.-S.; Talapin, D. V.; Segalman, R.; Majumdar, A. Enhanced Thermopower in PbSe Nanocrystal Quantum Dot Superlattices. *Nano Lett* **2008**, *8*, 2283–2288.
6. An, J. M.; Franceschetti, A.; Zunger, A. The Excitonic Exchange Splitting and Radiative Lifetime in PbSe Quantum Dots. *Nano Lett.* **2007**, *7*, 2129–2135.
7. Talapin, D. V.; Black, C. T.; Kagan, C. R.; Shevchenko, E. V.; Afzali, A.; Murray, C. B. Alignment, Electronic Properties, Doping, and On-Chip Growth of Colloidal PbSe Nanowires. *J. Phys. Chem. C* **2007**, *111*, 13244–13249.
8. Tuan, M.; Houtepen, A. J.; Schins, J. M.; Hanrath, T.; Piris, J.; Knulst, W.; Goossens, A. P. L. M.; Siebbeles, L. D. A. In Spite of Recent Doubts Carrier Multiplication Does Occur in PbSe Nanocrystals. *Nano Lett.* **2008**, *8*, 1713–1718.
9. Kamisaka, H.; Kilina, S. V.; Yamashita, K.; Prezhdo, O. V. *Ab Initio* Study of Temperature and Pressure Dependence of Energy and Phonon-Induced Dephasing of Electronic Excitations in CdSe and PbSe Quantum Dots. *J. Phys. Chem. C* **2008**, *112*, 7800–7808.
10. Tang, Z.; Kotov, N. A.; Giersig, M. Spontaneous Organization of Single CdTe Nanoparticles into Luminescent Nanowires. *Science* **2002**, *297*, 237–240.
11. Lifshitz, E.; Bashouti, M.; Kloper, V.; Kigel, A.; Eisen, M.; Berger, S. Synthesis and Characterization of PbSe Quantum Wires, Multipods, Quantum Rods, and Cubes. *Nano Lett.* **2003**, *3*, 857–862.
12. Zhuang, Q.; Liu, S.-J.; Yu, S.-H. Recent Advances in Oriented Attachment Growth and Synthesis of Functional Materials: Concept, Evidence, Mechanism, and Future. *J. Mater. Chem.* **2009**, *19*, 191–207.
13. Cho, K.-S.; Talapin, D. V.; Gaschler, W.; Murray, C. B. Designing PbSe Nanowires and Nanorings through Oriented Attachment of Nanoparticles. *J. Am. Chem. Soc.* **2005**, *127*, 7140–7147.
14. Klokkenburg, M.; Houtepen, A.; Koole, R.; De Folter, J. W.; Erné, B. H.; Van Faasen, E.; Vanmaekelbergh, D. Dipolar Structures in Colloidal Dispersions of PbSe and CdSe Quantum Dots. *Nano Lett.* **2007**, *7*, 2931–2936.
15. Van Huis, M. A.; Kunneman, L. T.; Overgaag, K.; Xu, Q.; Pandraud, G.; Zandbergen, H. W.; Vanmaekelbergh, D. Low-Temperature Nanocrystal Unification through Rotations and Relaxations Probed by *in-Situ* Transmission Electron Microscopy. *Nano Lett.* **2008**, *8*, 3959–3963.
16. Shim, M.; Guyot-Sionnest, P. Permanent Dipole Moment and Charges in Colloidal Semiconductor Quantum Dots. *J. Chem. Phys. C* **1999**, *111*, 6955–6964.
17. Talapin, D. V.; Shevchenko, E. V.; Murray, C. B.; Titov, A. V.; Král, P. Dipole—Dipole Interactions in Nanoparticle Superlattices. *Nano Lett.* **2007**, *7*, 1213–1219.
18. Walker, N. J.; Saunders, G. A.; Schäl, N. Acoustic Mode Vibrational Anharmonicity of PbSe and other IV—VI Compounds. *J. Phys. Chem. Solids* **1987**, *48*, 91–96.
19. Hinkel, V.; Haak, H.; Mariani, C.; Sorba, L.; Horn, K. Investigation of the Bulk Band Structure of IV—VI Compound Semiconductors: PbSe and PbTe. *Phys. Rev. B* **1989**, *40*, 5549–5556.
20. Hummer, K.; Grüneis, A.; Kresse, G. Structural and Electronic Properties of Lead Chalcogenides from First Principles. *Phys. Rev. B* **2007**, *75*, 195211.
21. Heda, N. L.; Rathor, A.; Sharma, V.; Ahmed, G.; Sharma, Y.; Ahuja, B. L. Study of Electronic Structure and Compton Profiles of PbS and PbSe. *J. Alloys Compd.* **2008**, *463*, 47–54.
22. Dargys, A. Spin Properties of Lead Chalcogenides in Absence of Magnetic Fields. *Phys. Scr.* **2006**, *74*, 519–524.
23. Kimura, K.; Nakajima, K.; Fujii, Y.; Mannami, M.-H. Observation of the PbSe(111) Surface Using High-Resolution Rutherford Backscattering Spectroscopy. *Surf. Sci.* **1994**, *318*, 363–367.
24. Moreels, I.; Fritzinger, B.; Martins, J. C.; Hens, Z. Surface Chemistry of Colloidal PbSe Nanocrystals. *J. Am. Chem. Soc.* **2008**, *130*, 15081–15086.
25. Ma, J.-X.; Jia, Y.; Song, Y.-L.; Liang, E.-J.; Wu, L.-K.; Wang, F.; Wang, X.-C.; Hu, X. The Geometric and Electronic Properties of the PbS, PbSe, and PbTe (001) Surfaces. *Surf. Sci.* **2004**, *551*, 91–98.
26. Meincke, H.; Ebling, D. G.; Heinze, J.; Tacke, M. Photoelectrochemical Study of Anodic Oxides on Lead Selenide Surfaces in Alkaline Solutions. *Fresenius' J. Anal. Chem.* **1999**, *365*, 147–149.
27. Semiletov, S. A.; Kudriavtseva, R. V.; Rakova, E. V. Surface Morphology and Structural Defects in Epitaxial Films. *Thin Solid Films* **1976**, *32*, 127–134.
28. Lüth, H. *Surfaces and Interfaces of Solid Materials,* 3rd ed.; Springer-Verlag: Berlin, 1997.
29. Wulff, G. Zur Frage der Geschwindigkeit des Wachsthums und der Auflösung der Krystallflachen. *Z. Kristallogr. Mineral.* **1901**, *34*, 449–530.
30. Houtepen, A. J.; Koole, R.; Vanmaekelbergh, D.; Meeldijk, J.; Hickey, S. G. The Hidden Role of Acetate in the PbSe Nanocrystal Synthesis. *J. Am. Chem. Soc.* **2006**, *128*, 6792–6793.
31. Dornhaus, R.; Nimtz, G.; Schlicht, B. *Narrow-Gap Semiconductors;* Springer-Verlag: Berlin, 1985.
32. Goniakowski, J.; Finocchi, F.; Noguera, C. Polarity of Oxide Surfaces and Nanostructures. *Rep. Prog. Phys.* **2008**, *71*, 016501.
33. Fang, C. M.; Parker, S. C.; De With, G. Atomistic Simulation of the Surface Energy of Spinel $MgAl_2O_4$. *J. Am. Ceram. Soc.* **2000**, *83*, 2082–2084.
34. Tasker, P. W. The Surface Energies, Surface Tensions, and Surface Structure of the Alkali Halide Crystals. *Phil. Mag. A* **1979**, *39*, 119–136.
35. Lawn, B. *Fracture of Brittle Solids,* 2nd ed.; Cambridge University Press: Cambridge, U.K., 1993.
36. Lorrain, P.; Corson, D. R.; Lorrain, F. *Electromagnetic Fields and Waves,* 3rd ed.; W. H. Freeman and Company: New York, 1988.
37. Kresse, G.; Hafner, J. *Ab Initio* Molecular Dynamics for Liquid Metals. *Phys. Rev. B* **1993**, *47*, 558–561.
38. Kresse, G.; Hafner, J. *Ab Initio* Molecular-Dynamics Simulation of the Liquid—Metal—Amorphous-Semiconductor Transition in Germanium. *Phys. Rev. B* **1994**, *49*, 14251–14269.
39. Kresse, G.; Furthmüller, J. Efficiency of *ab-Initio* Total Energy Calculations for Metals and Semiconductors Using a Plane-Wave Basis Set. *Comput. Mater. Sci.* **1996**, *6*, 15–50.
40. Blöchl, P. E. Projector Augmented-Wave Method. *Phys. Rev. B* **1994**, *50*, 17953–17979.
41. Kresse, G.; Furthmüller, J. Efficient Iterative Schemes for *ab Initio* Total-Energy Calculations Using a Plane-Wave Basis Set. *Phys. Rev. B* **1996**, *54*, 11169–11186.
42. Perdew, J. P.; Burke, K.; Ernzerhof, M. Generalized Gradient Approximation Made Simple. *Phys. Rev. Lett.* **1996**, *77*, 3865–3868.
43. Monkhorst, H. J.; Pack, J. D. Special Points for Brillouin-Zone Integrations. *Phys. Rev. B* **1976**, *13*, 5188–5192.